JOURNAL OF GEOPHYSICAL RESEARCH, VOL. 102, NO. D11, PAGES 12,819-12,829, JUNE 20, 1997

Temperature dependence of UV absorption cross sections and atmospheric implications of several alkyl iodides

Coleen M. Roehl,[1,2] James B. Burkholder,[3,4] Geert K. Moortgat,[1]
A. R. Ravishankara,[3,5] and Paul J. Crutzen[1]

Abstract. The ultraviolet absorption spectra of a number of alkyl iodides which have been found in the troposphere, CH_3I, C_2H_5I, $CH_3CH_2CH_2I$, CH_3CHICH_3, CH_2I_2, and CH_2ClI, have been measured over the wavelength range 200-380 nm and at temperatures between 298 and 210 K. The absorption spectra of the monoiodides CH_3I, C_2H_5I, $CH_3CH_2CH_2I$, and CH_3CHICH_3 are nearly identical in shape and magnitude and consist of single broad bands centered near 260 nm. The addition of a chlorine atom in CH_2ClI shifts its spectrum to longer wavelengths (σ_{max} at 270 nm). The spectrum of CH_2I_2 is further red-shifted, reaching a maximum of 3.85×10^{-18} cm^2 molecule^{-1} at 288 nm and exhibiting strong absorption in the solar actinic region, $\lambda > 290$ nm. Atmospheric photolysis rate constants, J values, have been calculated assuming quantum efficiencies of unity for different solar zenith angles as a function of altitude using the newly measured cross sections. Surface photolysis rate constants, calculated from the absorption cross sections measured at 298 K, range from 3×10^{-6} s^{-1} for CH_3I to 5×10^{-3} s^{-1} for CH_2I_2 at a solar zenith angle of 40°.

1. Introduction

Interest in atmospheric iodine has evolved out of a growing concern about the influence of halogen species on the ozone budget. Tropospheric [*Chameides and Davis*, 1980; *Jenkin et al.*, 1985; *Chatfield and Crutzen*, 1990; *Jenkin*, 1993; *Solomon et al.*, 1994a; *Davis et al.*, 1996] and stratospheric [*Solomon et al.*, 1994a] modeling efforts have suggested that iodine species play an important role in photochemical cycles involving ozone. Unlike the analogous chlorine or bromine species, the production of reactive iodine requires no complex heterogeneous mechanism since iodine-containing compounds are rapidly photodissociated. Atomic iodine, I, does not rapidly abstract hydrogen from saturated organic compounds, nor readily add to unsaturated compounds, and thus the reaction with ozone to generate IO radicals,

$$\text{(R1)} \qquad I + O_3 \rightarrow IO + O_2$$

appears to be the major I reaction in both the troposphere and the stratosphere.

When formed in the troposphere, IO will be photolyzed or alternatively will enter into catalytic sequences with NO, NO_2, and HO_2 forming $IONO_2$ and HOI reservoir species [*Wayne et al.*, 1995]. The potential effect of these cycles on the tropospheric ozone budget depends on the reservoir formation rates as well as their conversion rates back to active IO_X, the latter of which are not well established.

In order for I chemistry to contribute in the stratosphere, it is first necessary to transport these very photolytically active compounds to the upper atmosphere. The so-called "Staubsauger" mechanism or transport by convective clouds has been proposed as a possible means of rapidly carrying compounds from low altitudes to the upper troposphere or even lower stratosphere, particularly in the tropics [*Chatfield and Crutzen*, 1990]. When in the stratosphere, IO can react in simple destructive cycles with O_3 and O or in more complex cycles containing HO_2, ClO, BrO, or other IO radicals, analogous to the BrO_X and ClO_X reactions [*Solomon et al.*, 1994a; *Laszlo et al.*, 1995].

The largest, most easily quantified, and most studied source of atmospheric iodine is the photolysis of methyl iodide

$$\text{(R2)} \qquad CH_3I + h\nu \rightarrow CH_3 + I$$

Atmospheric measurements of CH_3I, primarily confined to the marine boundary layer, have yielded average mixing ratios of 1-4 parts per trillion by volume (pptv) [*Rasmussen et al.*, 1982; *Singh et al.*, 1983; *Reifenhäuser and Heumann*, 1992]. Elevated concentrations, as high as 43 pptv, have also been recorded in oceanic regions of high biogenic activity [*Oram and Penkett*, 1994]. An estimated 1-2 Tg yr^{-1} of iodine are thought to be released globally into the atmosphere following the photolysis of this alkyl iodide alone [*Davis et al.*, 1996], with an oceanic source contribution of 0.27-0.45 Tg yr^{-1} [*Singh et al.*, 1983].

Another iodine-containing species, CF_3I, considered a halon replacement, was recently investigated by *Solomon et al.* [1994b]. Photolytic release of I from CF_3I was found to be much faster than from CH_3I, with a lifetime in a sunlit atmosphere of less than a day. Although this result greatly limits the transport of CF_3I into the stratosphere and hence its effectiveness in stratospheric ozone destruction, tropospheric CF_3I could potentially produce significant quantities of I atoms.

[1]Max-Planck-Institut für Chemie, Atmospheric Chemistry Division, Mainz, Germany.
[2]Now at Chemical Kinetics and Photochemistry Group, Jet Propulsion Laboratory, Pasadena, California.
[3]Aeronomy Laboratory, NOAA, Boulder, Colorado.
[4]Also at Cooperative Institute for Research in Environmental Science, University of Colorado, Boulder.
[5]Also at Department of Chemistry and Biochemistry, University of Colorado, Boulder.

Paper number 97JD00530.
0148-0227/97/97JD-00530$09.00

Other iodine-containing compounds, CH_2I_2, CH_2ClI, C_2H_5I, CH_3CHICH_3, and $CH_3CH_2CH_2I$, which have recently been observed in seawater and marine air samples [*Class and Ballschmiter*, 1987, 1988; *Reifenhäuser and Heumann*, 1992; *Klick and Abrahamsson*, 1992; *Moore and Tokarczyk*, 1992; *Schall and Heumann*, 1993], have as of yet received no attention. In the study by *Schall and Heumann* [1993], especially high average concentrations of CH_3CHICH_3 were measured in the Arctic atmosphere (i.e., 2 pptv CH_3CHICH_3 as compared with 1.04 pptv CH_3I). Arctic seawater samples collected at different sites revealed similarly high concentrations of CH_2I_2 (1.65 ng L^{-1} in the middle of a fjord, 1.72 ng L^{-1} at a shore site, and 6.19 ng L^{-1} in a field of algae) and concentrations of CH_2ClI, CH_3CHICH_3, and $CH_3CH_2CH_2I$ which were comparable with the average CH_3I concentrations measured in the same respective sites (0.33, 0.59, and 1.03 ng L^{-1}).

Flux determinations, based on the surface-film model for gas exchange of *Liss and Slater* [1974], for the iodinated species studied here (other than CH_3I) have only appeared in two works. In the paper by *Moore and Tokarczyk* [1992] the maximum flux of CH_2ClI from the ocean to the atmosphere was estimated to be comparable with CH_3I. A similar calculation by *Klick and Abrahamsson* [1992] also approximated the flux of CH_2I_2, in high productivity areas, to be of the same order of magnitude as CH_3I. This would suggest that CH_3I is not necessarily always the most dominant iodine species in the marine atmosphere as previously assumed and indicates that other iodinated hydrocarbons than CH_3I must be taken into consideration for the global iodine budget.

The effect of these iodinated hydrocarbon emissions on the atmospheric iodine burden depends strongly on their photolysis rate constants, which in turn depend on their absorption cross sections. Using room temperature cross sections, *Solomon et al.* [1994a] calculated a globally averaged lifetime for CH_3I of about 4 days. However, as these authors also pointed out, lifetimes could be somewhat longer if the absorption cross sections in the long-wavelength region are temperature dependent. Although a number of spectral studies of CH_3I, C_2H_5I, CH_3CHICH_3, CH_2I_2, and CH_2ClI [*Porret and Goodeve*, 1938; *Haszeldine*, 1953; *Baughcum and Leone*, 1980; *Schmitt and Comes*, 1980, 1987; *Koffend and Leone*, 1981; *Phillips et al.*, 1992; *Jenkin et al.*, 1993; *Fahr et al.*, 1995; *Waschewsky et al.*, 1996] have appeared in the literature, measurements in the long-wavelength region of the spectra are sparse or nonexistent. Rigorous measurements of the absorption cross sections as a function of temperature, necessary for photolysis rate constant calculations at realistic atmospheric temperatures, have only been reported for CH_3I [*Fahr et al.*, 1995; *Waschewsky et al.*, 1996], but interpretations of even these results vary. *Waschewsky et al.* [1996] maintain that CH_3I dimers, formed at typical laboratory pressures, can measurably affect the temperature dependent shape of the CH_3I absorption spectrum and hence the atmospheric lifetime of CH_3I.

In this work, the temperature dependent absorption cross sections of CH_3I, C_2H_5I, $CH_3CH_2CH_2I$, CH_3CHICH_3, CH_2I_2, and CH_2ClI are reported. The atmospheric photolysis rate constants or J values of these compounds, which were calculated using the newly measured cross sections, are also presented as a function of altitude and solar zenith angle. Finally, the atmospheric implications of these photolysis rate constants are discussed.

2. Experimental Section

Absolute absorption cross section measurements were conducted at two separate laboratories, the Aeronomy Laboratory of NOAA in Boulder, Colorado and the Atmospheric Chemistry Division of the Max-Planck-Institut für Chemie (MPI) in Mainz, Germany, using very similar apparati. Detailed descriptions of the apparati, procedures, and data analyses used to measure the UV absorption spectra have previously been published [*Burkholder et al.*, 1993; *Maric et al.*, 1993] and hence will only be briefly mentioned here. Each apparatus was equipped with a deuterium (D_2) lamp, a jacketed glass cell with an optical path length between quartz inset windows of 100 cm (NOAA) and 63 cm (MPI), a spectrometer, and a photodiode array detector. Light from the D_2 lamp was passed through the cell and was focused onto the entrance slit of the spectrometer. The transmitted light was then detected by a 1024 pixel silicon diode array detector. The detectors were cooled to -30°C (MPI) and -40°C (NOAA) to reduce the dark current, and the wavelengths were calibrated (±0.2 nm) using the emission lines of a mercury Penray lamp. For $\lambda < 250$ nm a second calibration with a Zn-Cu hollow-cathode lamp was performed at MPI. Measurements were made at different temperatures between 298 and 210 K over the greatest range of pressures afforded by the particular vapor conditions and the maximum absorption in the spectral window. Typical cell pressures, measured with a 10 torr MKS pressure transducer, ranged between 0.05 and 10.0 torr. The cell temperatures were regulated by circulating cooled ethanol through the cell's jacket. Absorption measurements of CH_3I at 298, 275, 250, 225, and 210 K were made at NOAA. Spectral measurements of molecules C_2H_5I, $CH_3CH_2CH_2I$, CH_3CHICH_3, CH_2I_2, and CH_2ClI were performed at the MPI each at 298, 273, 248, and 223 K, with the exception of CH_2I_2, which due to its high freezing point (~279 K) could not be measured at 248 and 223 K.

The wavelength range encompassed in a single measurement segment (70 nm at MPI; 150 nm at NOAA) and the resolution (0.3 nm at MPI; 0.5 nm at NOAA) varied slightly between the two spectrometers. As expected, cross sections were found to be independent of resolution over the range of resolutions employed here. To cover the entire wavelength range between 200 and 380 nm, it was necessary to measure overlapping spectral regions and to splice the adjacent wavelength segments. The stability of the baseline was checked by extending measurements to wavelengths up to 420 nm, where no absorption should occur. A long-pass cutoff filter mounted between the light source and absorption cell was utilized (NOAA) for measurements at wavelengths longer than 280 nm to minimize photolysis of the sample in the absorption cell during the spectrum measurement. This precaution was not employed at MPI, since changes in absorption during the time period of the measurement were found to be less than the error in the measured absorbance.

The spectra were calculated from the Beer-Lambert's law,

$$\sigma(\lambda,T) = \ln\left[I_o(\lambda) / I(\lambda,T)\right] / lN \qquad (1)$$

where $\sigma(\lambda,T)$ represents the absorption cross section (in cm^2 $molecule^{-1}$) at wavelength λ and temperature T, l is the path length (in cm), N is the number density (in molecule cm^{-3}) of the species measured, and $I_o(\lambda)$ and $I(\lambda,T)$ are the transmitted light intensity measured with the cell evacuated and filled, re-

spectively. Absorption measurements were made by first measuring the unattenuated light level, $I_o(\lambda)$, passing through the absorption cell. The sample was then added to the cell and the pressure recorded. The attenuated light passing through the cell, $I(\lambda,T)$, was recorded. Typically, measurements consisted of 30-100 coadded scans of the detector with exposure times between 0.028 and 1.0 s. The absorption cell was evacuated, and the unattenuated light was recorded again. The values of $I_o(\lambda)$ measured before and after filling the absorption cell agreed within the stability of the lamp at all wavelengths. This method was repeated a minimum of 3 times for each temperature and spectral segment.

Uncertainties in the measured optical path length, temperature, pressure, sample purity, and absorbance contribute to the overall uncertainty in the measured absorption cross sections. The path length could be measured to better than 3 mm, which corresponds to a maximum error of 0.5%. At ambient temperature the accuracy of the temperature measurement is ~0.1%, but at lower temperatures, the uncertainty in the measurement of the temperature increases to almost 1%. The quoted uncertainties in the pressure measurements are less than 1%. As stated below, the purities of the samples are better than 99%, except for CH_2ClI, which had a given purity of better than 97%. The baseline fluctuations were < 0.1% as determined by measuring $I_o(\lambda)$ before filling and after pumping out the absorption cell. The precision of the absorbance measurements was ±2% RMS. We estimate the absolute uncertainty to be ±5% RMS at the peak of the spectra increasing to 10% in the wings.

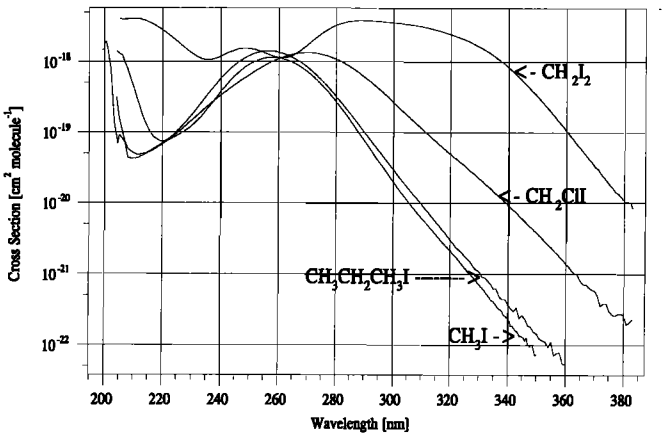

Figure 1. Absorption cross sections of CH_3I, $CH_3CH_2CH_2I$, CH_2I_2, and CH_2ClI as a function of wavelength at 298 K.

All samples, used in obtaining the results below, were degassed via freeze-thaw cycles at liquid N_2 temperature and vacuum distilled at temperatures just below their freezing points before use and were stored in darkened sample holders to prevent photodecomposition. No evidence of absorption due to impurities was observed in any sample investigated. In addition, CH_2I_2 was pretreated overnight with dry sodium thiosulfate and anhydrous calcium chloride and stored over copper to remove molecular iodine. The stated purities of the samples were CH_3I (> 99.5%), C_2H_5I (99%), $CH_3CH_2CH_2I$

Table 1. Absorption Cross Sections (in cm^2 $molecule^{-1}$) and Fitting Parameters a_1 (in K^{-1}) and a_2 (in K^{-2}) of CH_3I

λ, nm	σ, 298 K	σ, 275 K	σ, 250 K	σ, 225 K	σ, 210 K	a_1	a_2
200	1.81E-18	1.60E-18	1.35E-18	1.25E-18	1.18E-18	6.25E-3	2.62E-5
205	9.05E-20	7.44E-20	6.39E-20	5.97E-20	5.66E-20	8.43E-3	4.87E-5
210	4.27E-20	3.95E-20	3.92E-20	3.89E-20	3.89E-20	3.07E-3	2.42E-5
215	5.35E-20	4.99E-20	5.02E-20	5.02E-20	5.03E-20	2.61E-3	2.28E-5
220	6.92E-20	6.81E-20	6.74E-20	6.85E-20	6.92E-20	1.06E-3	1.22E-5
225	9.05E-20	8.84E-20	8.66E-20	8.84E-20	9.05E-20	1.74E-3	1.96E-5
230	1.24E-19	1.22E-19	1.19E-19	1.22E-19	1.24E-19	1.47E-3	1.67E-5
235	2.08E-19	2.03E-19	1.97E-19	2.02E-19	2.06E-19	1.91E-3	2.04E-5
240	3.79E-19	3.71E-19	3.62E-19	3.74E-19	3.81E-19	1.74E-3	2.06E-5
245	6.43E-19	6.34E-19	6.21E-19	6.49E-19	6.63E-19	1.52E-3	2.15E-5
250	9.30E-19	9.23E-19	9.12E-19	9.58E-19	9.82E-19	1.20E-3	2.11E-5
255	1.12E-18	1.12E-18	1.11E-18	1.17E-18	1.20E-18	8.90E-4	1.95E-5
260	1.13E-18	1.13E-18	1.12E-18	1.18E-18	1.21E-18	8.82E-4	1.93E-5
265	9.66E-19	9.57E-19	9.44E-19	9.91E-19	1.01E-18	1.21E-3	2.00E-5
270	7.09E-19	6.95E-19	6.76E-19	7.01E-19	7.14E-19	1.77E-3	2.11E-5
275	4.59E-19	4.42E-19	4.21E-19	4.29E-19	4.32E-19	2.52E-3	2.12E-5
280	2.69E-19	2.52E-19	2.34E-19	2.31E-19	2.30E-19	3.62E-3	2.24E-5
285	1.46E-19	1.33E-19	1.19E-19	1.13E-19	1.11E-19	4.84E-3	2.38E-5
290	7.54E-20	6.63E-20	5.75E-20	5.15E-20	5.00E-20	6.14E-3	2.57E-5
295	3.79E-20	3.24E-20	2.73E-20	2.32E-20	2.25E-20	7.27E-3	2.91E-5
300	1.98E-20	1.65E-20	1.42E-20	1.20E-20	1.17E-20	7.82E-3	3.53E-5
305	1.07E-20	8.92E-21	7.77E-21	6.65E-21	6.59E-21	7.82E-3	3.85E-5
310	6.03E-21	5.09E-21	4.49E-21	3.89E-21	3.89E-21	7.37E-3	3.71E-5
315	3.52E-21	3.00E-21	2.67E-21	2.32E-21	2.33E-21	6.98E-3	3.47E-5
320	2.12E-21	1.79E-21	1.58E-21	1.32E-21	1.35E-21	7.39E-3	3.54E-5
325	1.22E-21	1.03E-21	8.98E-22	7.29E-22	7.26E-22	7.23E-3	2.82E-5
330	7.24E-22	5.91E-22	4.98E-22	3.56E-22	3.86E-22	8.93E-3	3.74E-5
335	4.15E-22	3.27E-22	2.56E-22	1.67E-22	1.89E-22	0.01088	4.88E-5
340	2.25E-22	1.79E-22	1.33E-22	7.08E-23	9.15E-23	0.01130	4.46E-5
345	1.31E-22	9.19E-23	5.97E-23	3.36E-23	3.95E-23	0.01568	8.44E-5
350	7.38E-23	5.30E-23	3.00E-23	1.83E-23	1.87E-23	0.01594	8.22E-5

Read 1.81E-18 as 1.81×10^{-18}.

Table 2. Absorption Cross Sections (in cm^2 $molecule^{-1}$) and Fitting Parameters a_1 (in K^{-1}) and a_2 (in K^{-2}) of C_2H_5I

λ, nm	σ, 298 K	σ, 273 K	σ, 248 K	σ, 223 K	a_1	a_2
205	1.19E-19	9.89E-20	9.38E-20	8.20E-20	6.38E-3	3.15E-5
210	4.22E-20	4.01E-20	3.97E-20	4.44E-20	4.07E-3	6.28E-5
215	4.56E-20	4.13E-20	4.24E-20	4.54E-20	4.93E-3	6.57E-5
220	6.18E-20	5.65E-20	5.93E-20	6.24E-20	4.06E-3	5.70E-5
225	9.09E-20	8.47E-20	8.87E-20	9.06E-20	2.81E-3	3.81E-5
230	1.43E-19	1.35E-19	1.40E-19	1.45E-19	2.62E-3	3.83E-5
235	2.48E-19	2.39E-19	2.50E-19	2.53E-19	1.28E-3	2.17E-5
240	4.41E-19	4.32E-19	4.48E-19	4.59E-19	8.76E-4	1.96E-5
245	7.27E-19	7.26E-19	7.52E-19	7.79E-19	2.33E-4	1.62E-5
250	1.04E-18	1.05E-18	1.09E-18	1.14E-18	-1.11E-4	1.58E-5
255	1.25E-18	1.29E-18	1.33E-18	1.39E-18	-1.03E-3	6.06E-6
260	1.27E-18	1.32E-18	1.36E-18	1.41E-18	-1.48E-3	-3.32E-7
265	1.10E-18	1.13E-18	1.16E-18	1.19E-18	-1.09E-3	1.2E-11
270	8.35E-19	8.43E-19	8.54E-19	8.56E-19	-5.38E-4	-2.57E-6
275	5.63E-19	5.51E-19	5.43E-19	5.31E-19	7.70E-4	2.99E-7
280	3.46E-19	3.26E-19	3.15E-19	2.95E-19	2.01E-3	1.10E-6
285	1.97E-19	1.77E-19	1.66E-19	1.50E-19	3.85E-3	9.62E-6
290	1.06E-19	9.12E-20	8.28E-20	7.19E-20	5.47E-3	1.65E-5
295	5.54E-20	4.60E-20	4.01E-20	3.40E-20	7.00E-3	2.52E-5
300	2.85E-20	2.28E-20	1.97E-20	1.67E-20	8.56E-3	4.11E-5
305	1.47E-20	1.15E-20	9.88E-21	8.40E-21	9.31E-3	4.89E-5
310	8.04E-21	6.13E-21	5.30E-21	4.74E-21	0.01056	6.87E-5
315	4.29E-21	3.22E-21	2.79E-21	2.42E-21	0.01083	6.81E-5
320	2.36E-21	1.78E-21	1.54E-21	1.52E-21	0.01198	9.76E-5
325	1.33E-21	9.45E-22	8.91E-22	8.67E-22	0.01298	1.13E-4
330	8.05E-22	6.00E-22	5.71E-22		0.01456	1.75E-4
335	4.36E-22	2.98E-22	2.94E-22		0.01881	2.46E-4
340	2.82E-22	2.00E-22	1.50E-22		0.01390	9.08E-5
345	1.56E-22	1.04E-22	9.51E-23		0.01886	2.21E-4
350	1.08E-22	6.71E-23	5.34E-23		0.02019	2.01E-4
355	6.76E-23	6.24E-23	2.30E-23		-7.04E-3	-4.05E-4
360	4.95E-23	4.48E-23	2.04E-23		-4.32E-3	-3.22E-4
365	3.26E-23	1.07E-23	9.40E-24		0.03951	5.06E-4

Read 1.19E-19 as 1.19×10^{-19}.

(99%), CH_3CHICH_3 (99%), CH_2I_2 (99%), and CH_2ClI (97%). Two separate samples of CH_3I (at NOAA), and of C_2H_5I and CH_2ClI (at MPI) were used during the measurements with the results in excellent agreement.

3. Results and Discussion

UV Absorption Cross Sections

The continuous nature of the absorbances measured here is exemplified in Figure 1 in the spectra of CH_3I, $CH_3CH_2CH_2I$, CH_2I_2, and CH_2ClI, obtained at 298 K and over the wavelength range between 200 and 380 nm. Spectra of CH_2I_2 and CH_2ClI at 298 K recorded at NOAA were found to agree with the MPI spectra within the estimated uncertainty. However, only the MPI data are presented here since they should be more self-consistent with spectra for these same molecules measured (also at MPI) at the lower temperatures. The C_2H_5I and CH_3CHICH_3 spectra, which are not displayed in Figure 1 for the clarity reasons, are nearly identical to the CH_3I spectrum. Numerical values of the cross sections for all species are listed at 5 nm intervals in Tables 1-6. The magnitude and location of the maximum cross sections of the monoiodoalkanes are practically unaltered by an increase in the carbon chain length; $\sigma_{max}(CH_3I) = 1.15 \times 10^{-18}$ cm^2 $molecule^{-1}$ at 258 nm, $\sigma_{max}(C_2H_5I) = 1.29 \times 10^{-18}$ cm^2 $molecule^{-1}$ at 258 nm, $\sigma_{max}(CH_3CH_2CH_2I) = 1.42 \times 10^{-18}$ cm^2 $molecule^{-1}$ at 256 nm, and $\sigma_{max}(CH_3CHICH_3) = 1.48 \times 10^{-18}$ cm^2 $molecule^{-1}$ at 260 nm. The polyhaloalkane spectra, CH_2I_2 and CH_2ClI, are broader and have larger maximum cross sections than the analogous monosubstituted alkanes CH_3I or CH_3Cl ($\sigma_{max}(CH_2I_2) = 3.85 \times 10^{-18}$ cm^2 $molecule^{-1}$ at 288 nm and $\sigma_{max}(CH_2ClI) = 1.35 \times 10^{-18}$ cm^2 $molecule^{-1}$ at 270 nm). The broadening of the absorption regions of these higher halogen-substituted compounds has been attributed to the splitting of energy states from the halogen-halogen interactions [*Calvert and Pitts*, 1966]. As will be shown in the section on photodissociation rate constants, the location of a spectrum with respect to the solar actinic flux as well as the magnitude of the cross sections determines the atmospheric lifetimes of these species.

Comparisons of CH_3I, C_2H_5I, CH_3CHICH_3, CH_2I_2, and CH_2ClI with the only available data sets of 298 K measurements are shown in Figures 2-6. For every compound, the shape of the absorption features and the location of the maxima are in excellent agreement with previous data. Slight differences, clearly falling within the error limits, in the absolute values of the cross sections may have arisen from the extraction of the previous values from spectral plots. Only the CH_2I_2 data of *Schmitt and Comes* [1980] and *Koffend and Leone* [1981] and the CH_3I data of *Jenkin et al.* [1993] and *Fahr et al.* [1995] were tabulated rather than pictorially displayed. The maximum cross section of CH_2I_2 measured here is within 6% of the *Schmitt and Comes* [1980] data and 2% of *Koffend and Leone* [1981] data. Our CH_3I maximum cross

Table 3. Absorption Cross Sections (in cm^2 $molecule^{-1}$) and Fitting Parameters a_1 (in K^{-1}) and a_2 (in K^{-2}) of $CH_3CH_2CH_2I$

λ, nm	σ, 298 K	σ, 273 K	σ, 248 K	σ, 223 K	a_1	a_2
205	1.56E-19	1.25E-19	1.21E-19	1.04E-19	7.60E-3	4.37E-5
210	5.05E-20	4.74E-20	5.50E-20	5.27E-20	2.83E-4	1.57E-5
215	5.14E-20	5.03E-20	5.43E-20	4.93E-20	-1.49E-3	-2.46E-5
220	6.84E-20	6.80E-20	7.06E-20	6.44E-20	-1.59E-3	-2.97E-5
225	1.04E-19	1.03E-19	1.05E-19	9.78E-20	-8.91E-4	-2.14E-5
230	1.77E-19	1.76E-19	1.76E-19	1.69E-19	-3.75E-4	-1.26E-5
235	3.28E-19	3.27E-19	3.26E-19	3.16E-19	-3.11E-4	-1.04E-5
240	5.81E-19	5.85E-19	5.88E-19	5.80E-19	-6.11E-4	-8.04E-6
245	9.19E-19	9.35E-19	9.44E-19	9.46E-19	-8.49E-4	-6.09E-6
250	1.24E-18	1.27E-18	1.30E-18	1.31E-18	-1.22E-3	-6.11E-6
255	1.41E-18	1.45E-18	1.50E-18	1.51E-18	-1.55E-3	-7.76E-6
260	1.36E-18	1.39E-18	1.43E-18	1.44E-18	-1.44E-3	-8.67E-6
265	1.13E-18	1.15E-18	1.16E-18	1.15E-18	-1.02E-3	-1.04E-5
270	8.22E-19	8.19E-19	8.14E-19	7.86E-19	-3.06E-4	-1.16E-5
275	5.34E-19	5.19E-19	5.03E-19	4.67E-19	5.24E-4	-1.50E-5
280	3.20E-19	3.01E-19	2.82E-19	2.48E-19	1.68E-3	-1.66E-5
285	1.81E-19	1.64E-19	1.48E-19	1.24E-19	3.08E-3	-1.44E-5
290	9.96E-20	8.53E-20	7.48E-20	6.23E-20	5.56E-3	8.12E-6
295	5.42E-20	4.55E-20	3.89E-20	3.29E-20	6.76E-3	2.05E-5
300	2.96E-20	2.47E-20	2.13E-20	1.85E-20	7.16E-3	2.90E-5
305	1.63E-20	1.38E-20	1.20E-20	1.08E-20	6.90E-3	3.20E-5
310	9.45E-21	7.87E-21	7.18E-21	6.49E-21	7.10E-3	4.01E-5
315	5.32E-21	4.67E-21	4.20E-21	3.92E-21	5.59E-3	2.78E-5
320	3.01E-21	2.67E-21	2.52E-21	2.16E-21	3.68E-3	1.40E-7
325	1.77E-21	1.55E-21	1.42E-21	1.20E-21	4.23E-3	2.38E-7
330	1.10E-21	8.71E-22	8.11E-22		0.01140	1.23E-4
335	6.27E-22	4.81E-22	5.37E-22		0.01576	2.58E-4

Read 1.56E-19 as 1.56×10^{-19}.

Table 4. Absorption Cross Sections (in cm^2 $molecule^{-1}$) and Fitting Parameters a_1 (in K^{-1}) and a_2 (in K^{-2}) of CH_3CHICH_3

λ, nm	σ, 298 K	σ, 273 K	σ, 248 K	σ, 223 K	a_1	a_2
205	4.49E-19	2.91E-19	2.16E-19	1.49E-19	0.01514	8.46E-5
210	4.53E-20	3.79E-20	3.63E-20	3.69E-20	7.84E-3	7.23E-5
215	3.57E-20	3.19E-20	3.18E-20	3.25E-20	4.96E-3	5.08E-5
220	4.20E-20	4.05E-20	4.01E-20	4.01E-20	1.55E-3	1.27E-5
225	6.45E-20	6.17E-20	6.06E-20	6.10E-20	2.21E-3	1.99E-5
230	1.10E-19	1.07E-19	1.06E-19	1.08E-19	1.60E-3	1.80E-5
235	2.04E-19	2.04E-19	2.01E-19	2.05E-19	4.80E-4	6.81E-6
240	3.82E-19	3.88E-19	3.87E-19	3.95E-19	-3.33E-4	1.21E-6
245	6.67E-19	6.83E-19	6.86E-19	7.06E-19	-6.80E-4	9.47E-7
250	1.02E-18	1.05E-18	1.06E-18	1.10E-18	-7.95E-4	2.89E-6
255	1.33E-18	1.37E-18	1.41E-18	1.47E-18	-9.66E-4	5.70E-6
260	1.48E-18	1.53E-18	1.58E-18	1.65E-18	-1.14E-3	5.12E-6
265	1.43E-18	1.46E-18	1.50E-18	1.56E-18	-5.89E-4	8.24E-6
270	1.20E-18	1.22E-18	1.23E-18	1.26E-18	-4.39E-4	2.81E-6
275	9.02E-19	8.90E-19	8.85E-19	8.92E-19	7.92E-4	8.73E-6
280	6.14E-19	5.93E-19	5.68E-19	5.55E-19	1.65E-3	4.66E-6
285	3.86E-19	3.62E-19	3.33E-19	3.15E-19	2.88E-3	5.34E-6
290	2.26E-19	2.06E-19	1.80E-19	1.64E-19	4.13E-3	5.59E-6
295	1.28E-19	1.12E-19	9.33E-20	8.11E-20	5.71E-3	1.04E-5
300	6.94E-20	5.85E-20	4.70E-20	3.97E-20	7.20E-3	1.93E-5
305	3.73E-20	3.03E-20	2.41E-20	1.93E-20	8.19E-3	2.33E-5
310	2.04E-20	1.62E-20	1.30E-20	1.02E-20	8.75E-3	2.81E-5
315	1.09E-20	8.67E-21	7.10E-21	5.34E-21	8.49E-3	2.25E-5
320	6.27E-21	4.80E-21	3.52E-21	2.75E-21	0.01079	4.36E-5
325	3.48E-21	2.71E-21	2.06E-21		9.54E-3	2.76E-5
330	2.02E-21	1.54E-21	1.21E-21		0.01099	5.94E-5
335	1.15E-21	8.49E-22	6.57E-22		0.01237	7.58E-5
340	6.88E-22	5.05E-22	4.27E-22		0.01369	1.22E-4
345	4.02E-22	2.81E-22	2.46E-22		0.01632	1.71E-4
350	2.53E-22	1.75E-22	1.75E-22		0.01850	2.47E-4
355	1.50E-22	1.00E-22	9.56E-23		0.01941	2.43E-4
360	1.05E-22	6.53E-23	4.39E-23		0.01861	1.39E-4
365	6.66E-23	3.80E-23	5.20E-23		0.02985	5.09E-4
370	4.79E-23	2.63E-23	5.07E-23		0.03724	7.68E-4
375	5.35E-23	3.14E-23	6.33E-23		0.03671	8.07E-4
380	5.30E-23	3.71E-23	4.77E-23		0.02200	4.00E-4

Read 4.49E-19 as 4.49×10^{-19}.

Table 5. Absorption Cross Sections of CH_2I_2 (in cm^2 $molecule^{-1}$)

λ, nm	σ, 298 K	σ, 273 K	λ, nm	σ, 298 K	σ, 273 K
205	4.07E-18	3.69E-18	295	3.75E-18	3.78E-18
210	4.04E-18	3.91E-18	300	3.59E-18	3.60E-18
215	3.66E-18	3.64E-18	305	3.39E-18	3.38E-18
220	2.77E-18	2.77E-18	310	3.15E-18	3.13E-18
225	1.93E-18	1.93E-18	315	2.81E-18	2.79E-18
230	1.31E-18	1.30E-18	320	2.45E-18	2.42E-18
235	1.07E-18	1.04E-18	325	2.04E-18	2.02E-18
240	1.20E-18	1.18E-18	330	1.62E-18	1.61E-18
245	1.47E-18	1.46E-18	335	1.21E-18	1.19E-18
250	1.53E-18	1.52E-18	340	8.34E-19	8.02E-19
255	1.34E-18	1.29E-18	345	5.33E-19	5.00E-19
260	1.15E-18	1.09E-18	350	3.24E-19	2.96E-19
265	1.25E-18	1.21E-18	355	1.88E-19	1.68E-19
270	1.75E-18	1.75E-18	360	1.06E-19	9.15E-20
275	2.54E-18	2.59E-18	365	5.85E-20	4.92E-20
280	3.30E-18	3.40E-18	370	3.30E-20	2.75E-20
285	3.76E-18	3.86E-18	375	1.83E-20	1.43E-20
290	3.84E-18	3.93E-18	380	1.14E-20	8.86E-21

Read 4.07E-18as 4.07×10^{-18}.

section is within 6% of the *Jenkin et al.* [1993] value, but 17% lower than that reported by *Fahr et al.* [1995] at 295 K and 260 nm. The CH_2ClI spectrum deduced from *Schmitt and Comes'* [1987] plot was scaled to their quoted maximum, which is 11% larger than our CH_2ClI maximum; no error limits were given for this value. *Haszeldine* [1953] reported only the cross section maxima for CH_3I and C_2H_5I in the gas phase, and these values fall 23% and 8% below ours. No spectral information of gas phase $CH_3CH_2CH_2I$ was found.

The effect of temperature on the absorption cross sections is shown for CH_3I and CH_2I_2 in Figures 7 and 8. The spectra demonstrate typical temperature dependencies [*Hubrich and*

Table 6. Absorption Cross Sections (in cm^2 $molecule^{-1}$) and Fitting Parameters a_1 (in K^{-1}) and a_2 (in K^{-2}) of CH_2ClI

λ, nm	σ, 298 K	σ, 273 K	σ, 248 K	σ, 223 K	a_1	a_2
205	1.32E-18	1.36E-18	1.28E-18	1.20E-18	-1.59E-3	-3.83E-5
210	4.21E-19	3.37E-19	2.87E-19	2.41E-19	8.47E-3	3.76E-5
215	1.11E-19	9.66E-20	8.94E-20	8.68E-20	6.12E-3	4.30E-5
220	7.50E-20	7.39E-20	7.51E-20	7.40E-20	2.32E-4	1.29E-6
225	9.76E-20	9.85E-20	9.94E-20	1.01E-19	-9.38E-5	6.60E-6
230	1.49E-19	1.50E-19	1.51E-19	1.52E-19	-2.68E-4	-1.4E-11
235	2.28E-19	2.31E-19	2.31E-19	2.32E-19	-5.12E-4	-3.88E-6
240	3.36E-19	3.43E-19	3.42E-19	3.44E-19	-7.93E-4	-6.64E-6
245	4.78E-19	4.90E-19	4.88E-19	4.92E-19	-9.29E-4	-7.58E-6
250	6.58E-19	6.78E-19	6.75E-19	6.78E-19	-1.22E-3	-1.13E-5
255	8.82E-19	9.10E-19	9.09E-19	9.17E-19	-1.25E-3	-9.98E-6
260	1.11E-18	1.15E-18	1.16E-18	1.17E-18	-1.56E-3	-1.14E-5
265	1.29E-18	1.32E-18	1.35E-18	1.37E-18	-1.05E-3	-2.94E-6
270	1.35E-18	1.39E-18	1.42E-18	1.44E-18	-1.33E-3	-5.93E-6
275	1.27E-18	1.30E-18	1.33E-18	1.35E-18	-1.07E-3	-2.98E-6
280	1.09E-18	1.10E-18	1.12E-18	1.12E-18	-6.18E-4	-3.09E-6
285	8.44E-19	8.47E-19	8.47E-19	8.38E-19	-3.26E-4	-5.54E-6
290	6.04E-19	5.99E-19	5.82E-19	5.67E-19	3.00E-4	-7.11E-6
295	4.12E-19	3.97E-19	3.76E-19	3.59E-19	1.55E-3	-2.45E-6
300	2.67E-19	2.52E-19	2.34E-19	2.18E-19	2.38E-3	-4.73E-7
305	1.71E-19	1.59E-19	1.45E-19	1.35E-19	3.13E-3	3.94E-6
310	1.11E-19	1.03E-19	9.40E-20	8.70E-20	3.13E-3	3.03E-6
315	7.30E-20	6.78E-20	6.25E-20	5.67E-20	2.74E-3	-3.17E-6
320	4.90E-20	4.57E-20	4.25E-20	3.85E-20	2.44E-3	-5.33E-6
325	3.32E-20	3.05E-20	2.89E-20	2.62E-20	2.87E-3	1.40E-6
330	2.20E-20	2.04E-20	1.93E-20	1.52E-20	8.52E-4	-4.21E-5
335	1.44E-20	1.32E-20	1.24E-20	1.02E-20	2.02E-3	-2.25E-5
340	9.34E-21	8.39E-21	7.97E-21		5.20E-3	4.54E-5
345	5.93E-21	5.14E-21	4.86E-21		7.05E-3	6.88E-5
350	3.75E-21	3.17E-21	3.14E-21		9.12E-3	1.17E-4
355	2.33E-21	1.89E-21	2.00E-21		0.01227	1.89E-4

Read 1.32E-18 as 1.32×10^{-18}.

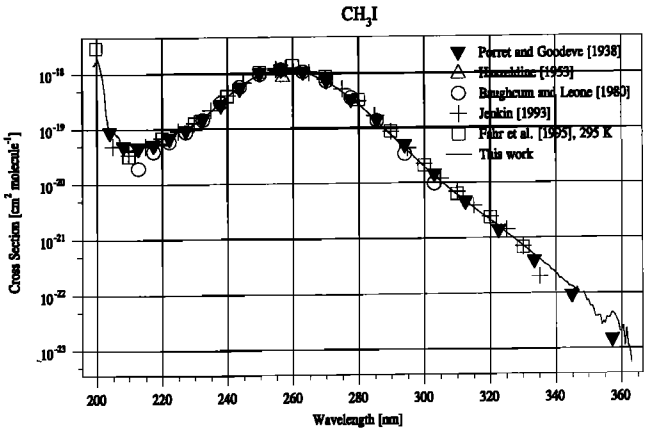

Figure 2. Absorption spectrum of CH_3I at 298 K measured in this work (solid line) and in previous studies: *Porret and Goodeve* [1938] (inverted triangles), *Haszeldine* [1953] (upward triangles), *Baughcum and Leone* [1980] (circles), *Jenkin et al.* [1993] (pluses), and *Fahr et al.* [1995] (squares).

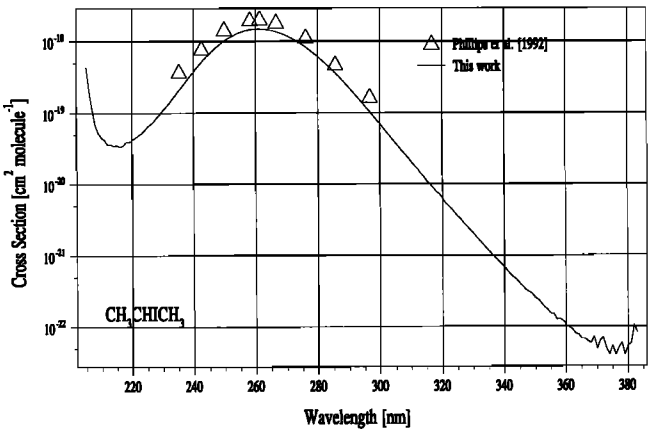

Figure 4. Absorption spectrum of CH_3CHICH_3 at 298 K measured in this work (solid line) and by *Phillips et al.* [1992] (triangles).

Stuhl, 1980; *Simon et al.*, 1988; *Gillotay and Simon*, 1989; *Burkholder et al.*, 1993, 1994; *Fahr et al.*, 1995]; the cross sections in the long-wavelength tail of the absorption band increase with increasing temperature, while the band maximum decreases. The integrated cross-sectional area of a particular molecule varied less than 2% in going from one temperature to the next. Similar temperature trends were observed for the other species, as can be seen in Tables 1-6. Also included in Tables 1-4 and 6 are the results, a_1 and a_2 from second-order polynomial fits of the temperature dependent cross section data. The simple analytical expression for the temperature dependence is given by

$$\sigma(\lambda,T) = \sigma(\lambda,298\text{ K})\begin{bmatrix}1+a_1(T-298\text{ K})\\+a_2(T-298\text{ K})\end{bmatrix} \quad (2)$$

Although this formula has no real physical basis, this parameterization does reproduce the observed temperature dependence and allows for interpolation to other temperatures.

As indicated by Figure 6 of *Waschewsky et al.* [1996], their long-wavelength (290 nm < λ < 320 nm) CH_3I cross sections also increase with increasing temperature, however, they attribute this change to the formation of CH_3I dimers. Using the K_{eq} calculated by *Waschewsky et al.* [1996], a change in our CH_3I calculated cross sections of ~30% would be expected over the pressure range used; this was not observed and, in fact, changes were less than 5%. Using the dimer interpretation, the shape of the CH_3I spectra beyond 290 nm is also not expected to change with temperature (i.e., assuming that only monomer is present.) We observe a change in the shape of the spectra as the temperature is decreased. Finally, no deviation from Beer-Lambert's law is observed at any wavelength for our CH_3I, which means that the measured absorbance is linear with pressure or absorber concentration. It seems unlikely that the product of the cross section and concentration of the dimer would exactly equal that for the monomer at all wavelengths. Conducting absorption cross section measurements under the low-pressure conditions (pressure < 0.1 torr) which *Waschewsky et al.* [1996] consider safe from dimer effects would be difficult, since a path length ~100 m would be re-

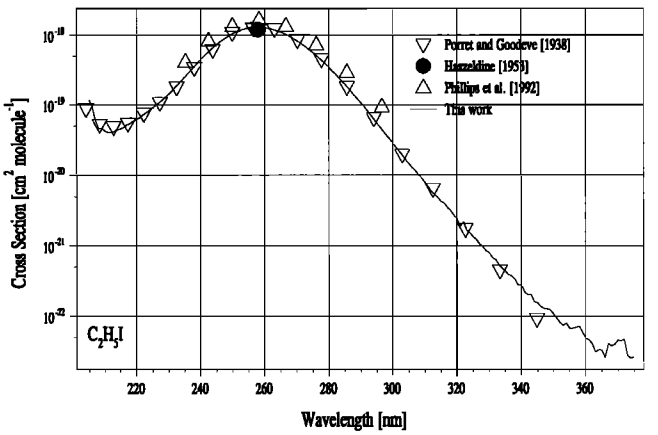

Figure 3. Absorption spectrum of C_2H_5I at 298 K measured in this work (solid line) and in previous studies: *Porret and Goodeve* [1938] (inverted triangles), *Haszeldine* [1953] (circles), and *Phillips et al.* [1992] (triangles).

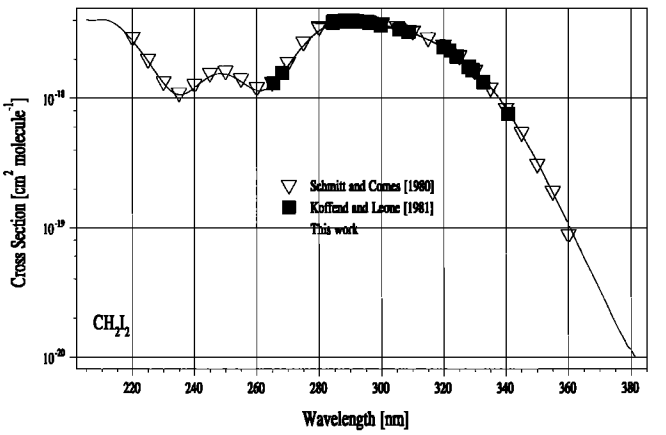

Figure 5. Absorption spectrum of CH_2I_2 at 298 K measured in this work (solid line) and in previous studies: *Schmitt and Comes* [1980] (inverted triangles) and *Koffend and Leone* [1981] (squares).

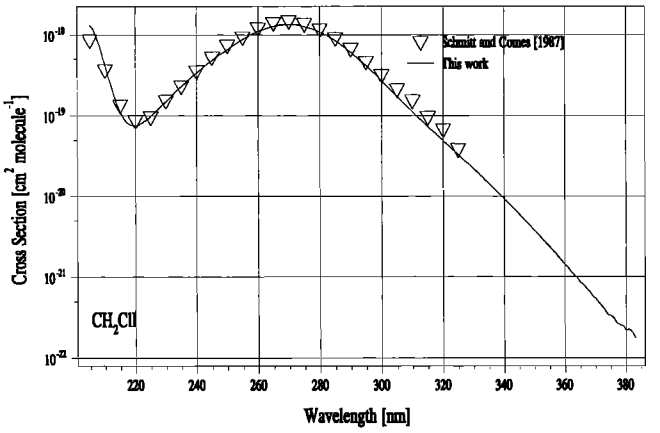

Figure 6. Absorption spectrum of CH_2ClI at 298 K measured in this work (solid line) and by *Schmitt and Comes* [1987] (triangles).

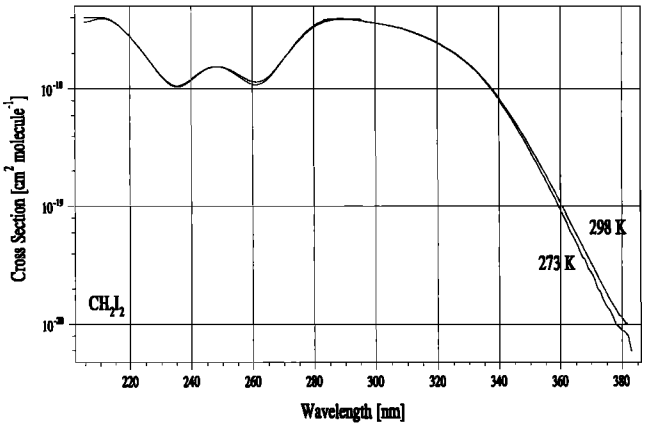

Figure 8. Absorption cross sections of CH_2I_2 versus wavelength as a function of temperature.

quired for a decent signal to noise ratio. It can therefore only be said that the experimental results of this study do not support the dimer formation interpretation.

Photodissociation Rate Constant Calculations and Atmospheric Implications

In order to assess the atmospheric importance of these alkyl iodides, atmospheric photodissociation rate constants $J(\theta,z)$ were calculated employing the relationship:

$$J(\theta,z) = \int \sigma(\lambda)\phi(\lambda)I(\lambda,\theta,z)d\lambda \qquad (3)$$

where $\sigma(\lambda)$ is the absorption cross section as a function of wavelength λ, $\phi(\lambda)$ is the quantum yield for photodissociation, and $I(\lambda,\theta,z)$ is the actinic flux as a function of wavelength λ, solar zenith angle θ, and altitude z. The high-resolution cross section data obtained in this study at the various temperatures were first reduced to a resolution of 1 nm and then used as input. Quantum efficiencies for photodissociation of unity were assumed, in accord with what has been observed in photolysis experiments of CH_2ClI or CH_2I_2 at wavelengths greater than about 200 nm [*Baughcum and Leone*, 1980; *Schmitt and Comes*, 1980, 1987]. J values were evaluated with the LUTHER program, which was developed at the MPI and is based on the radiation transfer model by *Luther and Gelinas* [1976]. This program calculates the solar flux by simulating multiple scattering and atmospheric absorption due to O_2, O_3, and NO_2 and subsequently determines the integral by summing up over the wavelength range 200-380 nm with 1.0 nm increments. The recommended O_2, O_3, and NO_2 absorption cross section data of the *World Meteorological Organization* (*WMO*) [1985] and a globally averaged albedo value of 0.3 were employed.

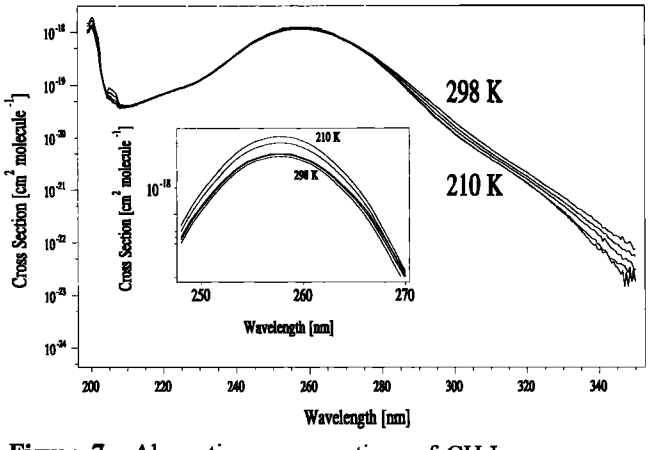

Figure 7. Absorption cross sections of CH_3I versus wavelength as a function of temperature.

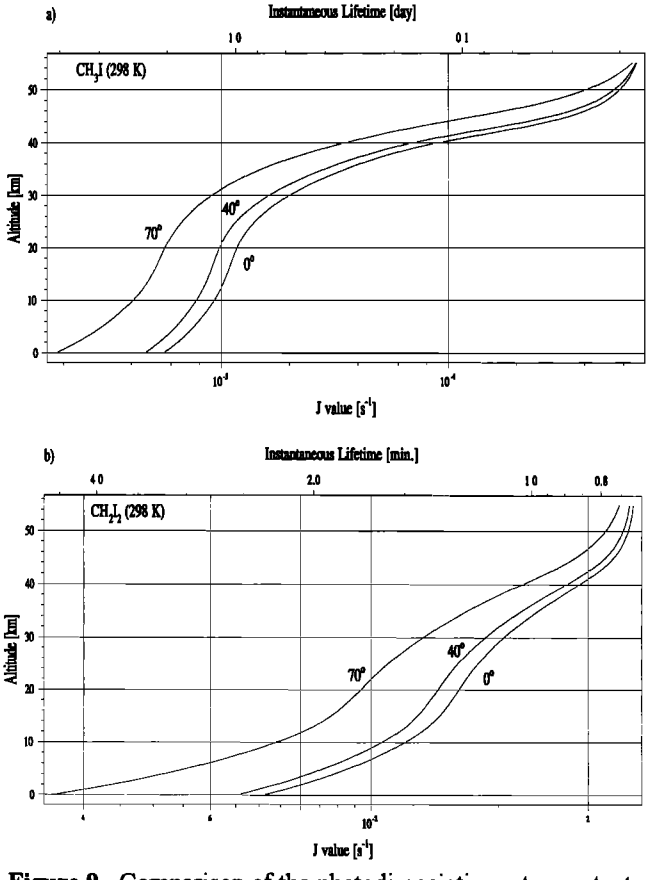

Figure 9. Comparison of the photodissociation rate constants as a function of altitude for various solar zenith angles for (a) CH_3I and (b) CH_2I_2 calculated with the spectra obtained at 298 K.

J values were calculated for all molecules at different solar zenith angles (0°, 10°, 20°, 30°, 40°, 50°, 60°, 70°, 78°, and 86°) using the 298 K absorption cross sections measured here. Plots of the J values versus altitude for selected solar zenith angles, 0°, 40°, and 70°, are shown in Figure 9 for the molecules CH_3I and CH_2I_2. Instantaneous lifetimes were calculated as the inverse of the photolysis rate constants and are plotted along the upper x axis. Diurnally averaged J values will, of course, lead to lifetimes which are a factor of 2 to 3 longer. As expected, the photodissociation rate constants increase (or the instantaneous lifetimes decrease) with decreasing solar zenith angles and increasing altitudes for both CH_3I and CH_2I_2. J values ranging from (1.8-5.5) x 10^{-6} s^{-1} were obtained for CH_3I at the surface in going from 70° to 0°, which correspond to instantaneous lifetimes of 6.3 and 2.1 days, respectively. The slower increase in CH_3I J values at the lower altitudes as opposed to the higher altitudes results from the presence of O_3. Ozone in the upper atmosphere absorbs most of the radiation at $\lambda < 290$ nm, so photolysis of CH_3I in the lower atmosphere is limited to the spectral region > 290 nm. As was shown in Figure 2, the absorption cross sections of CH_3I drop off very quickly at $\lambda > 290$ nm and therefore the J values at the lower altitudes increase slowly. This is in contrast to the J values for CH_2I_2, which increase at approximately the same rate at all altitudes. Since the CH_2I_2 spectrum is red-shifted relative to CH_3I, more of it lies above the 290 nm ozone cutoff, and therefore CH_2I_2 is not so strongly affected by the ozone absorbance. Note also that the photolysis rate constants calculated for CH_2I_2 are much larger than for CH_3I. Surface values range from (3.6-7.1) x 10^{-3} s^{-1}, yielding instantaneous lifetimes of 4.6 and 2.3 min! The accelerated photolysis rate constants of CH_2I_2 are a result of the greater overlap of the solar flux and the absorption spectrum.

The effect of solar flux and absorption spectrum overlap is also clearly demonstrated in Figure 10, where the results from calculations performed at a solar zenith angle of 40° for all species are displayed. The enhancement of the photodissociation rate constants in going from CH_3I to CH_2I_2 directly correlates to the shift of the related spectrum to longer wavelengths.

The effect of the temperature dependency of the cross sections on the calculated J values was explored through additional J values calculations utilizing the cross sections measured at lower temperatures for only the two extreme cases, CH_3I and CH_2I_2. These results, obtained at solar zenith angles of 40° and up to altitudes of 15 km, are exhibited in Figure 11. As seen in both plots, a decrease in the long-wavelength absorption tail due to lowering the temperature acts to reduce the corresponding J values. For the same reason as discussed above, the photolysis rate constants of CH_3I are more strongly affected by this shift in the absorption spectra than those of CH_2I_2. The photodissociation rate constant of CH_3I at the surface decreases by ~17% in going from 298 to 275 K and drops nearly a factor of 2 by 225 K. In contrast, a decline of less than 3% was calculated for the surface CH_2I_2 J values in going from 298 to 273 K.

Since atmospheric temperatures vary with altitude, photolysis rates calculated from cross sections measured at only one temperature are only reasonable if the temperature dependency of the J values is weak, as is the case for CH_2I_2. The J value curves in Figure 11b are therefore good representations of the atmospheric photolysis rates for CH_2I_2. For the strongly temperature dependent CH_3I, the atmospheric J values are not well represented by any of the single temperature curves shown in Figure 11a, and the actual climatological temperature profile must be incorporated. The temperature dependencies of the J values were first determined for each altitude in 1 km intervals using Figure 11a data. J values were then calculated for each altitude from these relationships at the corresponding atmospheric temperature [*WMO*, 1985]

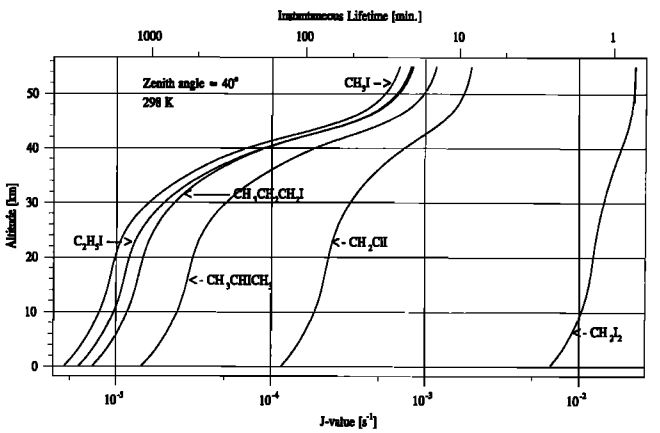

Figure 10. Comparison of the photodissociation rate constants of all species studied here as a function of altitude for a solar zenith angle of 40° calculated with the spectra obtained at 298 K.

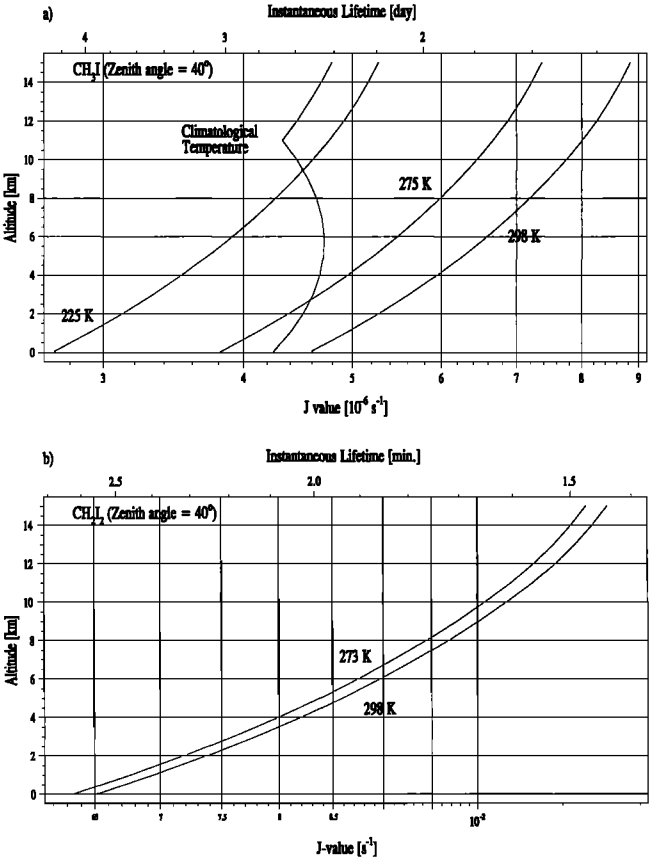

Figure 11. Comparison of the photodissociation rate constants calculated at solar zenith angles of 40° with the spectra obtained at various temperatures for (a) CH_3I and (b) CH_2I_2 as a function of altitude.

and are plotted in Figure 11a. Considering that the atmospheric temperature decreases with increasing altitude, one might expect the J values to decrease with altitude. This is not the case, however, since the solar flux increases with height and thus accelerates the photolysis. This solar flux induced increase in the J values is almost directly compensated for by the effect of the decreasing temperature in the troposphere, and the resultant J value curve is nearly independent of altitude, remaining almost constant from the surface to the tropopause. Although they were not calculated, the temperature dependencies of the J values for the other monoiodides are expected to be comparable to that of CH_3I since their spectra so closely resemble that of CH_3I, and similar temperature dependencies in their absorption cross sections were observed.

Without a more sophisticated model, it is not possible to determine globally averaged lifetimes for these species. However, all of the alkyl iodides are very short-lived, and the effect of the temperature on the calculated photolysis rate constants is greatest for the monoiodoalkanes. As was true with CF_3I, the short photolysis lifetimes of these species greatly restrict any transport into the stratosphere and hence their effectiveness in stratospheric ozone depletion. Although gas phase observations of these alkyl iodides is limited, the existing studies do agree that ocean to air fluxes are large. This, coupled with the large photodissociation rate constants, suggests that alkyl halides, especially CH_2ClI and CH_2I_2, are significant sources of reactive iodine in the marine troposphere, notably in the polar regions at large solar zenith angles. (The dihalogenated compounds are the shortest-lived species of those measured and are capable of releasing two reactive halogens into the atmosphere [*Baughcum and Leone*, 1980; *Schmitt and Comes*, 1980, 1987; *Fenter et al.*, 1993].) Further observations of the alkyl iodides, focusing on the strong seasonal and geographic variations in the source strength, are still necessary however. Likewise, information on the reactive iodine species obtained either through indirect observations of reservoir species or through direct observation of IO in the atmosphere is needed. Clearly, a better understanding of both the sources and the sinks is crucial to determining a reliable iodine budget and its influence on tropospheric ozone.

4. Conclusions

A complete set of temperature dependent absorption cross sections for CH_3I, C_2H_5I, $CH_3CH_2CH_2I$, CH_3CHICH_3, CH_2I_2, and CH_2ClI has been measured for the first time and has been used in calculations of the atmospheric photodissociation rate constants. The CH_2I_2 and CH_2ClI molecules absorb strongly at wavelengths greater than 290 nm, overlapping significantly with the solar spectrum and hence yielding large photodissociation rate constants. Because of the location and magnitude of its spectrum, small changes in the absorption cross sections of the CH_3I due to temperature strongly influenced the photodissociation rate constant calculations. Tropospheric photolysis appears to be the major atmospheric loss process for all of these alkyl halides.

Acknowledgments. Research at MPI was funded through the Max-Planck-Gesellschaft. The work at NOAA was funded in part by NASA's Upper Atmospheric Research Program.

References

Baughcum, S. L., and S. R. Leone, Photofragmentation infrared emission studies of vibrationally excited free radicals CH_3 and CH_2I, *J. Chem. Phys., 72*, 6531-6545,1980.

Burkholder, J. B., R. K. Talukdar, A. R. Ravishankara, and S. Solomon, Temperature dependence of the HNO_3 UV absorption cross sections, *J. Geophys. Res., 98*, 22,937-22,948, 1993.

Burkholder, J. B., R. K. Talukdar, and A. R. Ravishankara, Temperature dependence of the $ClONO_2$ UV absorption spectrum, *Geophys. Res. Lett., 21*, 585-588, 1994.

Calvert, J. G., and J. N. Pitts Jr., *Photochemistry*, pp. 522-528, John Wiley, New York.,1966.

Chameides, W. L., and D. D. Davis, Iodine: Its possible role in tropospheric photochemistry, *J. Geophys. Res., 85*, 7383-7398, 1980.

Chatfield, R. B., and P. J. Crutzen, Are there interactions of iodine and sulfur species in marine air photochemistry?, *J. Geophys. Res., 95*, 22,319-22,341, 1990.

Class, T., and K. Ballschmiter, Chemistry of organic traces in air, IX, Evidence of natural marine sources for chloroform in regions of high primary production, *Fresenius Z. Anal. Chem., 327*, 40-41, 1987.

Class, T., and K. Ballschmiter, Chemistry of organic traces in air, VIII, Sources and distributions of bromo- and bromochloromethanes in marine air and surface waters of the Atlantic Ocean, *J. Atmos. Chem., 6*, 35-46, 1988.

Davis, D., J. Crawford, S. Liu, S. McKeen, A. Bandy, D. Thornton, F. Rowland, and D. Blake, Potential impact of iodine on tropospheric levels of ozone and other critical oxidizing species, *J. Geophys. Res., 101*, 2135-2147, 1996.

Fahr, A., A. K. Nayak, and M. J. Kurylo, The ultraviolet absorption cross sections of CH_3I temperature dependent gas and liquid phase measurements, *Chem. Phys., 197*, 195-203, 1995.

Fenter, F. F., P. D. Lightfoot, F. Caralp, R. Lesclaux, J. T. Niranen, and D. Gutman, Kinetics of the $CHCl_2$ and CH_2Cl association reactions with molecular oxygen between 298 and 448 K and from 1 to 760 torr of total pressure, *J. Phys. Chem., 97*, 4695-4703, 1993.

Gillotay, D., and P. C. Simon, Ultraviolet absorption spectrum of trifluoro-bromo-methane and difluoro-bromo-chloro-methane in the vapour phase, *J. Atmos. Chem., 8*, 41-62, 1989.

Haszeldine, R. N., Studies in spectroscopy, III, The ultra-violet absorption spectra of halogen-containing aliphatic iodo-compounds, and the relative stability of free halogen containing alkyl radicals, *J. Chem. Soc.*, 1764-1771, 1953.

Hubrich, C., and F. Stuhl, The ultraviolet absorption of some halogenated methanes and ethanes of atmospheric interest, *J. Photochem., 12*, 93-107, 1980.

Jenkin, M. E., A comparative assessment of the role of iodine photochemistry in the tropospheric ozone depletion, in *The Tropospheric Chemistry of Ozone in the Polar Regions*, NATO ASI Ser., vol. I7, edited by H. Niki and K.-H. Becker, pp. 405-416, Springer-Verlag, New York, 1993.

Jenkin, M. E., R. A. Cox, and D. E. Candeland, Photochemical aspects of tropospheric iodine behaviour, *J. Atmos. Chem., 2*, 359-375, 1985.

Jenkin, M. E., T. P. Murrells, S. J. Shalliker, and G. D. Hayman, Kinetics and product study of the self-reactions of allyl and allyl peroxy radicals at 296 K, *J. Chem. Soc. Faraday Trans., 89*, 433-446, 1993.

Klick, S., and K. Abrahamsson, Biogenic volatile iodated hydrocarbons in the ocean, *J. Geophys. Res., 97*, 12,683-12,687, 1992.

Koffend, J. B., and S. R. Leone, Tunable laser photodissociation: Quantum yield of $I^*(^2P_{1/2})$ from CH_2I_2, *Chem. Phys. Lett., 81*, 136-141, 1981.

Laszlo, B., M. J. Kurylo, and R. E. Huie, Absorption cross sections, kinetics of formation, and self-reaction of the IO radical produced via laser photolysis of $N_2O/I_2/N_2$ mixtures, *J. Phys. Chem., 99*, 11,701-11,707, 1995.

Liss, P. S., and P. G. Slater, Flux of gases across the air-sea interface, *Nature, 247*, 181-184, 1974.

Luther, F. M., and R. J. Gelinas, Effect of molecular multiple scattering and surface albedo on atmospheric photodissociation rates, *J. Geophys. Res., 81*, 1125-1132, 1976.

Maric, D., J. P. Burrows, R. Meller, and G. K. Moortgat, A study of

the UV/Vis spectrum of molecular chlorine, *J. Photochem. Photobiol. A, 70*, 205-214, 1993.

Moore, R. M., and R. Tokarczyk, Chloro-iodomethane in N. Atlantic waters: A potentially significant source of atmospheric iodine, *Geophys. Res. Lett., 19*, 1779-1782, 1992.

Oram, D. E., and S. A. Penkett, Observations in Eastern England of elevated methyl iodide concentrations in air of Atlantic Ocean, *Atmos. Environ., 28*, 1159-1174, 1994.

Phillips, D. L., A. B. Myers, and J. J. Valentini, Investigations of solvation effects on short-time photodissociation dynamics of alkyl iodides, *J. Phys. Chem., 96*, 2039-2044, 1992.

Porret, D., and C. F. Goodeve, The continuous absorption spectra of alkyl iodides and alkyl bromides and their quantal interpretation, *Proc. R. Soc. London A, 165*, 31-42, 1938.

Rasmussen, R. A., M. A. K. Khalil, R. Gunawardena, and S. D. Hoyt, Atmospheric methyl iodide (CH_3I), *J. Geophys. Res., 87*, 3086-3090, 1982.

Reifenhäuser, W., and K. G. Heumann, Determinations of methyl iodide in the Antarctic atmosphere and the south polar sea, *Atmos. Environ., 26A*, 2905-2912, 1992.

Schall, C., and K. G. Heumann, GC determinations of volatile organoiodine and organobromine compounds in Arctic seawater and air samples, *Fresenius J. Anal. Chem., 346*, 717-722, 1993.

Schmitt, G., and F. J. Comes, Photolysis of CH_2I_2 and 1,1-$C_2H_4I_2$ at 300 nm, *J. Photochem., 14*, 107-123, 1980.

Schmitt, G., and F. J. Comes, Competitive photodecomposition reactions of chloroiodomethane, *J. Photochem. Photobiol. A,, 41*, 13-30, 1987.

Simon, P. C., D. Gillotay, N. Vanlaethem-Meuree, and J. Wisemberg, Ultraviolet absorption cross-sections of chloro- and chlorofluoromethanes at stratospheric temperatures, *J. Atmos. Chem., 7*, 107-135, 1988.

Singh, H. B., L. J. Salas, and R. E. Stiles, Methyl halides in and over the eastern Pacific (40°N-32°S), *J. Geophys. Res., 88*, 3684-3690, 1983.

Solomon, S., R. R. Garcia, and A. R. Ravishankara, On the role of iodine in ozone depletion, *J. Geophys. Res., 99*, 20,491-20,499, 1994a.

Solomon, S., J. B. Burkholder, A. R. Ravishankara, and R. R. Garcia, Ozone depletion and global warming of CF_3I, *J. Geophys. Res., 99*, 20,929-20,935, 1994b.

Waschewsky, G. C. G., R. Horansky, and V. Vaida, Effect of dimers on the temperature-dependent absorption cross section of methyl iodide, *J. Phys. Chem., 100*, 11,559-11,565, 1996.

Wayne, R. P., *et al.*, Halogen oxides: Radicals, sources, and reservoirs in the laboratory and in the atmosphere, *Atmos. Environ., 29*, 121-127, 1995.

World Meteorological Organization (WMO), Atmospheric ozone: 1985, Global Ozone Research and Monitoring Project,WMO Rep. 16, Geneva, 1985.

J. B. Burkholder and A. R. Ravishankara, Aeronomy Laboratory, NOAA, 325 Broadway, Boulder, CO 80303. (e-mail: burk@al.noaa.gov)

P. J. Crutzen and G. K. Moortgat, Max-Planck-Institut fur Chemie, Atmospheric Chemistry Division, Postfach 3060, 55020 Mainz, Germany. (e-mail: moo@diane.mpch-mainz.mpg.de)

C. M. Roehl, Jet Propulsion Laboratory, California Institute of Technology, M/S 183-901, 4800 Oak Grove Drive, Pasadena, CA 91109. (e-mail: croehl@ftuvs.jpl.nasa.gov)

(Received November 14, 1996; revised February 12, 1997;
accepted February 12, 1997.)